Supporting Information

Stringing MOF-Derived Nanocages Strategy for Enhanced Oxygen Evolution Reactions

Huajie Xu,[ab] Yiwei Yang,[a] Xiaoxi Yang,[a] Jing Cao,*[a] Weisheng Liu, [a] and Yu Tang*[a]

[a] State Key Laboratory of Applied Organic Chemistry, Key Laboratory of Nonferrous Metal Chemistry and Resources Utilization of Gansu Province, College of Chemistry and Chemical Engineering, Lanzhou University, Lanzhou 730000, People's Republic of China

[b] School of Chemical and Material Engineering, Fuyang Normal University, Fuyang 236037, People's Republic of China

*Email: tangyu@lzu.edu.cn, caoj@lzu.edu.cn

Contents

5. Supplementary Tables

1. Experimental section

1.1 Preparation of CeO_2 nanorods (CeO_2NRs) and CeO_2 nanoparticles (CeO_2 NPs)

Typically, 4 mmol cerium(III) nitrate hexahydrate and different moles of sodium dihydrogen phosphate dehydrate (0.01 mmol, 0.05 mmol, 0.1 mmol, and 0.2 mmol) were dissolved in 15 mL distilled water. After being stirred at room temperature for 60 min, the mixed solution was transferred into a 20 mL Teflon-lined stainless autoclave and heated at 200°C for 144 h under autogenous pressure and static conditions in an electric oven. Upon leaving the solution cool to room temperature, the precipitates were separated by centrifuging, washed with distilled water and ethanol three times in turn, and then dried at 60℃ for 1 day.

2 mmol $Ce(NO_3)_3 \cdot 6H_2O$ was dissolved in 40 mL deionized water. Then, 2.5 mL of ammonia was added, and stirred for 30 min at room temperature, followed by being transferred to a 50 mL Teflon-lined stainless-steel autoclave. The autoclave was sealed and placed in an oven at 180 °C for 6 h and then cooled down naturally, and the precipitates were harvested by several rinsing-centrifugation cycles with deionized (DI) water and ethanol and then dried at 50 °C.

1.2 Preparation of the ZIF-67@CeO_2NR Templates

8.6 milligrams of the different length of CeO_2 nanorods was redispersed in 20 mL of ethanol under sonication for 30 min to obtain a homogeneous solution. 1 g of polyvinylpyrrolidone (PVP, average mol. wt. 40000) was added to the solution while stirring. A quarter later, the methanol solution of cobalt nitrate hexahydrate (0.873 g, 5 mL) was added drop by drop. On the other hand, 2-Methylimidazole (0.984 g) was dissolved in methanol (5 mL) to generate another clear solution. Then, the two solutions were mixed rapidly together. The mixture was kept still at room temperature for 12 h. After that, the precipitates were collected, separated by centrifugation, washed carefully with methanol, and dried at 80 °C overnight.

1.3. Preparation of the CoS@CeO_2NR

Twenty-five milligrams of ZIF-67@CeO_2NR was redispersed in 20 mL of ethanol under sonication for 30 min to obtain a homogeneous solution, then 0.2 g of

thioacetamide was added to the solution while stirring. The mixture was kept at 90 °C for 1 h. After being cooled to room temperature naturally, the black precipitates were harvested by several rinsing-centrifugation cycles with deionized (DI) water and ethanol and then dried at 50 °C.

1.4. Preparation of CeO_x/CoS@CeO_2NR

0.18 g of CoS@CeO_2NR was first dispersed in 15 mL of absolute ethyl alcohol, and after 30 mins of sonication, a homogeneous slurry was formed, followed by the addition of 0.15 mmol of hexamethylenetetramine (HMT) and 0.05 mmol $Ce(NO_3)_3 \cdot 6H_2O$. The mixture was kept stirring for 30 mins at room temperature, followed by being transferred to a 50 mL Teflon-lined stainless-steel autoclave. The autoclave was sealed and placed in an oven at 180 °C for 6 h and then cooled down naturally, and the precipitates were harvested by several rinsing-centrifugation cycles with deionized (DI) water and ethanol and then dried at 50 °C.

1.5. Preparation of hollow CeO_x/CoS

Preparation of CeO_x/CoS is similar with CeO_x/CoS@CeO_2NR, and only the CeO_2 nanorods were not added in the synthesis of ZIF-67.

2. Materials characterization.

Transmission electron microscopy (TEM), high-resolution transmission electron microscopy (HRTEM) and elemental mapping were performed on a JEOL JEM 2100 TEM (200kV). Scanning electron microscopy was performed on Carl Zeiss. The chemical compositions were investigated by energy dispersive X-ray spectroscopy (EDX). X-ray diffraction (XRD) patterns were collected on an X'Pert ProX-ray diffractometer with Cu Kα radiation (λ = 0.1542 nm) (40 kV and 40 mA). X-ray photoelectron spectroscopy (XPS) spectra were recorded on a VG ESCALAB 220I-XL device and corrected using C1s line at 284.6 eV. The Brunauer-Emmett-Teller (BET) specific surface area was determined using N_2 adsorption–desorption on an Autosorb-IQ2-MPC system, and the pore size distribution was computed based on quenched solid density functional theory using the adsorption branch. The Raman spectra were obtained with a Horiba Raman spectrometer model via using a 532 nm line of Ar^+ ion laser as the excitation source at room temperature.

3. Electrochemical measurement.

Electrochemical measurements were carried out in a typical three-electrode glass cell connected to a CHI 760E Electrochemical Workstation (CHI Instruments, Shanghai Chenhua Instrument Corp., China), comprising a platinum foil counter electrode, a saturated Hg/HgO reference electrode, and a glassy carbon working electrode coated with electrocatalysts. The catalysts were uniformly cast onto a glassy carbon electrode with a total loading of 200 μg cm^{-2}. Before each test, the working electrode was fabricated as follows. 5.0 mg electrocatalysts were first dispersed in 0.95 mL ethanol, and then 0.05 mL Nafion solution (5.0 wt%) was added, followed by 1.0 h sonication. 10.0 μL suspension was pipetted onto a glassy carbon electrode, which was mechanically polished and ultrasonically washed in advance. Ultimately, the working electrode was prepared after solvent evaporation in air for 10.0 min. All potentials were calculated with respect to reversible hydrogen electrode (RHE) based on: E (RHE) = E (Hg/HgO) + 0.059 × pH + 0.098 V. The overpotential (η) was calculated by η (V) = E (RHE) - 1.23V. Linear sweep voltammetry (LSV) and cyclic voltammetry (CV) measurements were recorded at a scan rate of 1 mV s^{-1}. The potential was calibrated with respect to a reversible hydrogen electrode (RHE) in 1 M KOH solution. 1M KOH solution was bubbled for about fifteen minutes to saturate it before each test. The ECSA was measured by cyclic voltammetry (CV) using the same working electrodes at a potential window of 0.2-0.4 V *vs*. RHE in 1 M aqueous KOH solution. CV curves were obtained at different scan rates of 50, 100, 150, 200, 250, and 300 mV s^{-1}. After plotting charging current density differences ($\Delta J = J_a - J_c$ at the potential of 0.3 V) versus the scan rates, the slope, twice of the double-layer capacitance C_{dl}, is used to represent the ECSA. To test the stability of catalysts, a galvanostatic measurement at a fixed current density (J) of 10 mA cm^{-2} was performed. AC impedance spectroscopy was acquired in a frequency range from 100 kHz to 0.1 Hz at amplitude of 10 mV.

4. Supplementary Figures

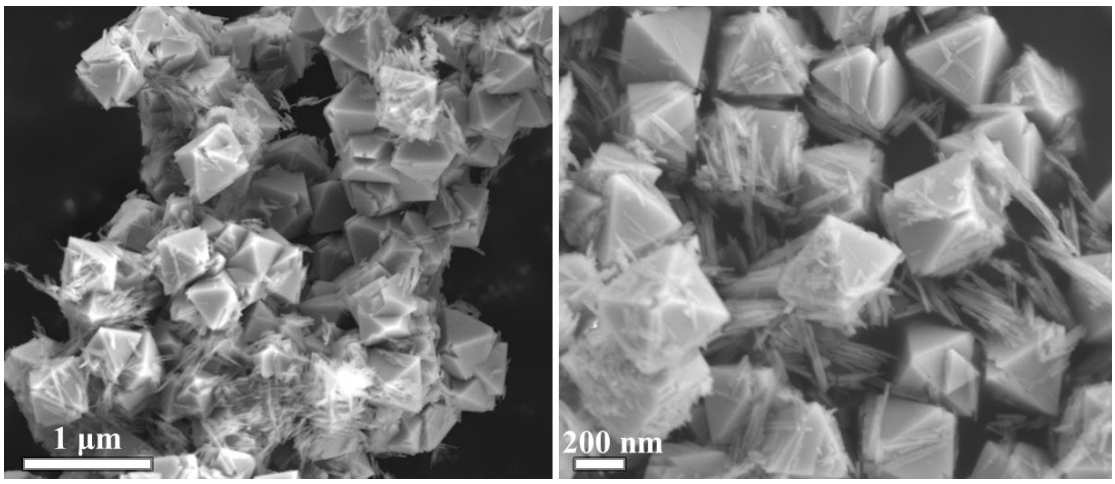

Fig. S1. The SEM image for CeO_2 nanorods with 0.01 mM of sodium dihydrogen phosphate dehydrate.

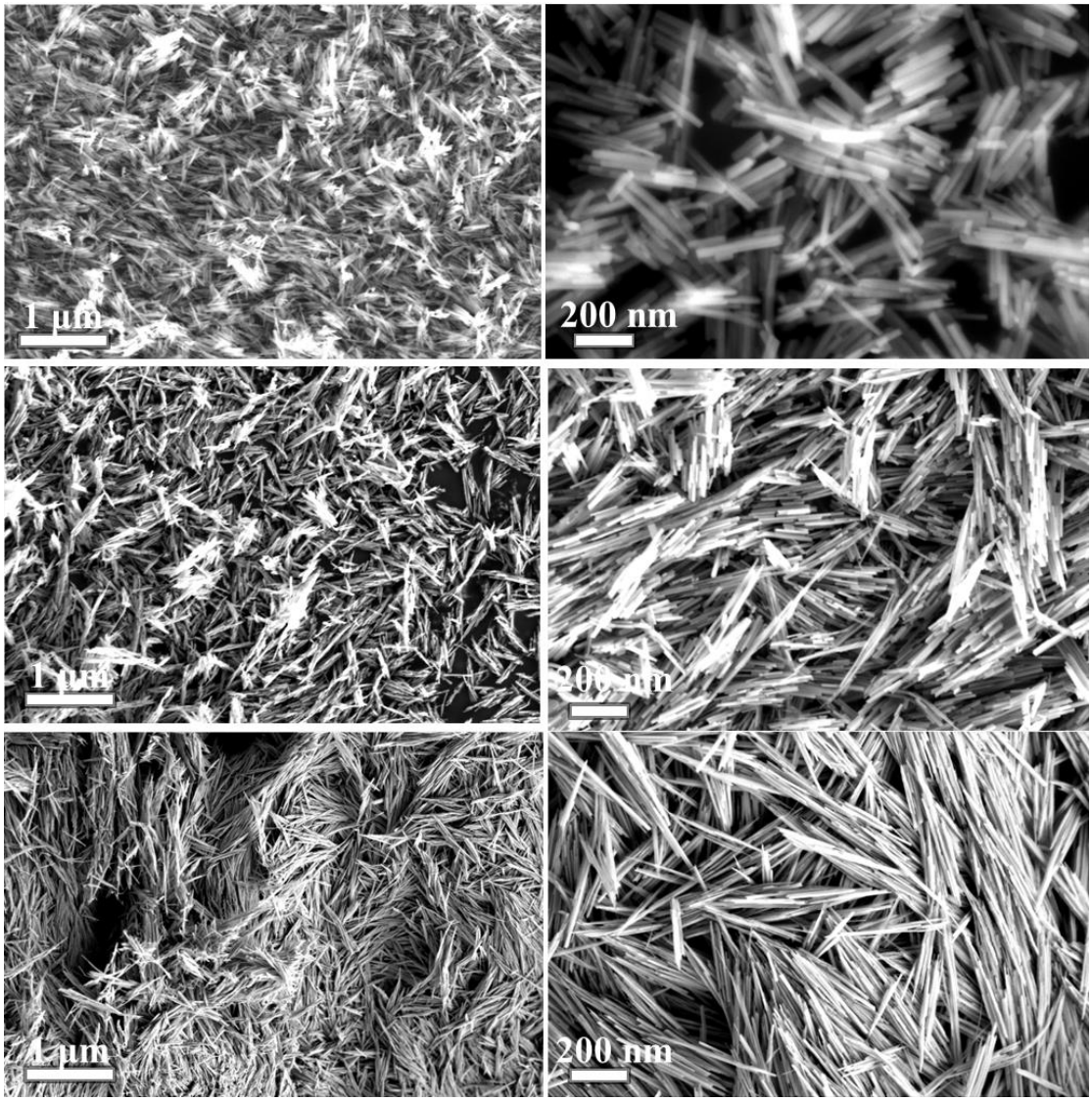

Fig. S2. The SEM image for CeO_2 nanorods with 0.05 mM, 0.1 mM and 0.2 mM of sodium dihydrogen phosphate dehydrate.

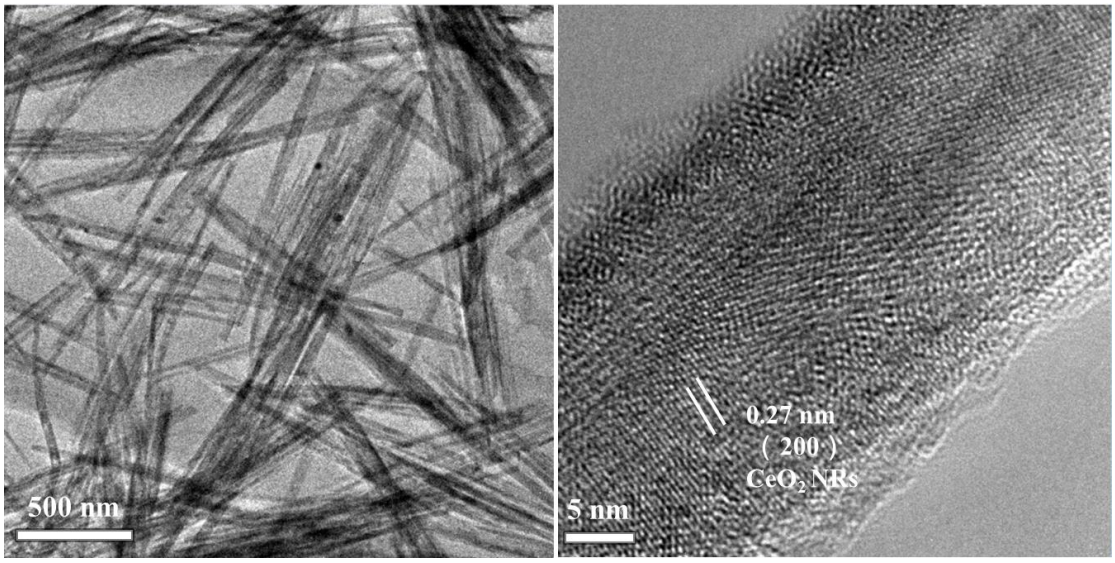

Fig. S3. The TEM image for CeO_2 nanorods with 0.2 mM of sodium dihydrogen phosphate dehydrate.

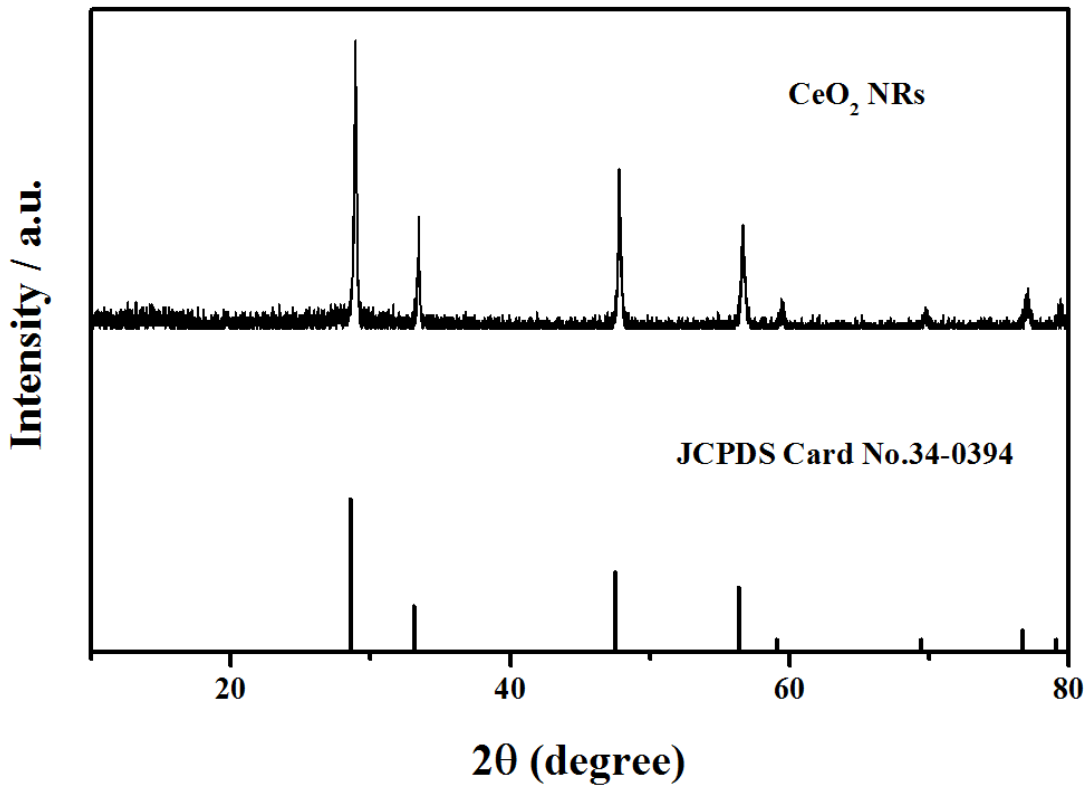

Fig. S4. XRD patterns for CeO_2 nanorods with 0.2 mM of sodium dihydrogen phosphate dehydrate.

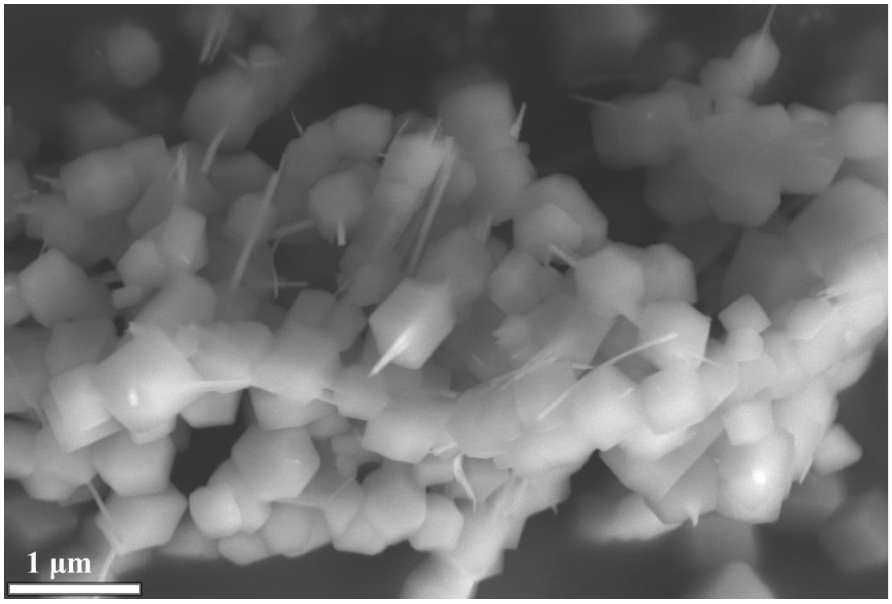

Fig. S5. The SEM image for ZIF-67@L-CeO_2NRs.

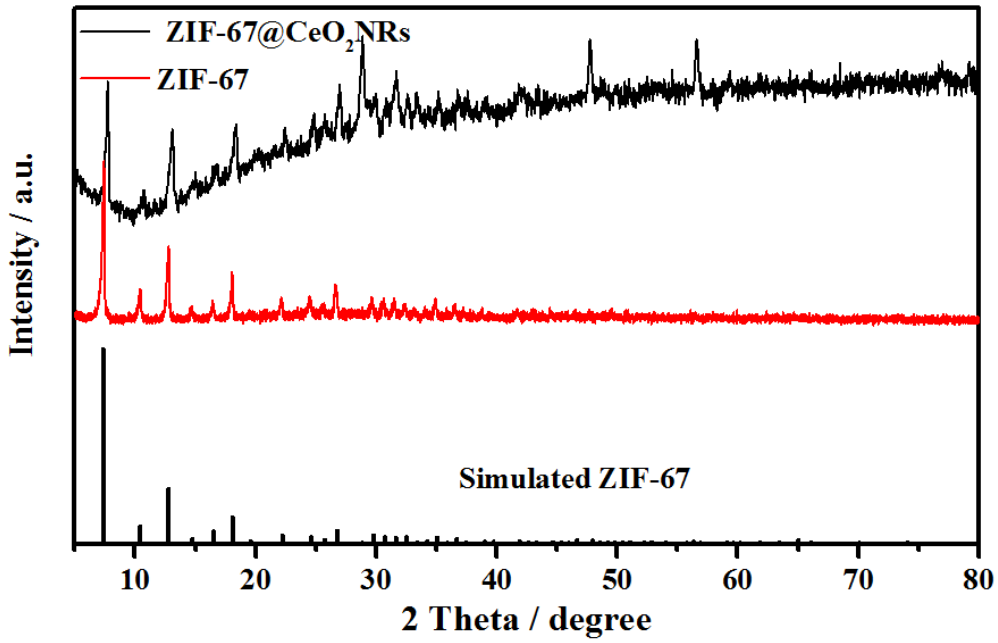

Fig. S6. XRD patterns of ZIF-67 and ZIF-67@L-CeO_2NRs.

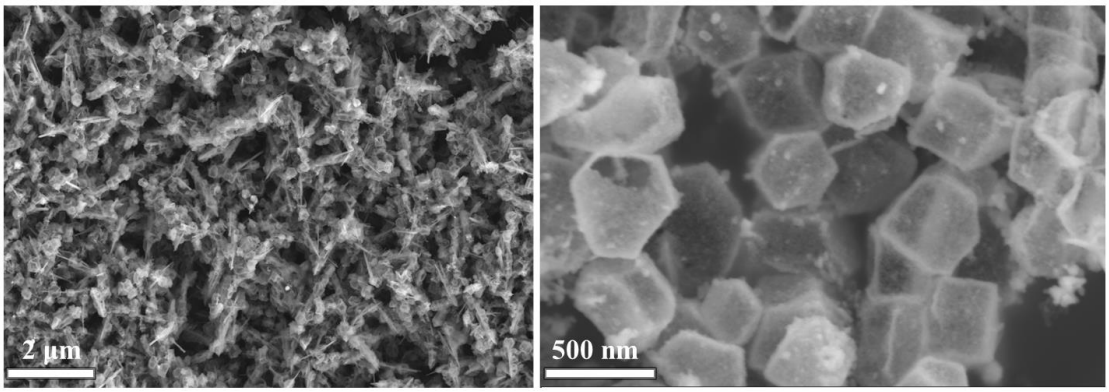

Fig. S7. The SEM image for CeO_x/CoS@L-CeO_2NRs.

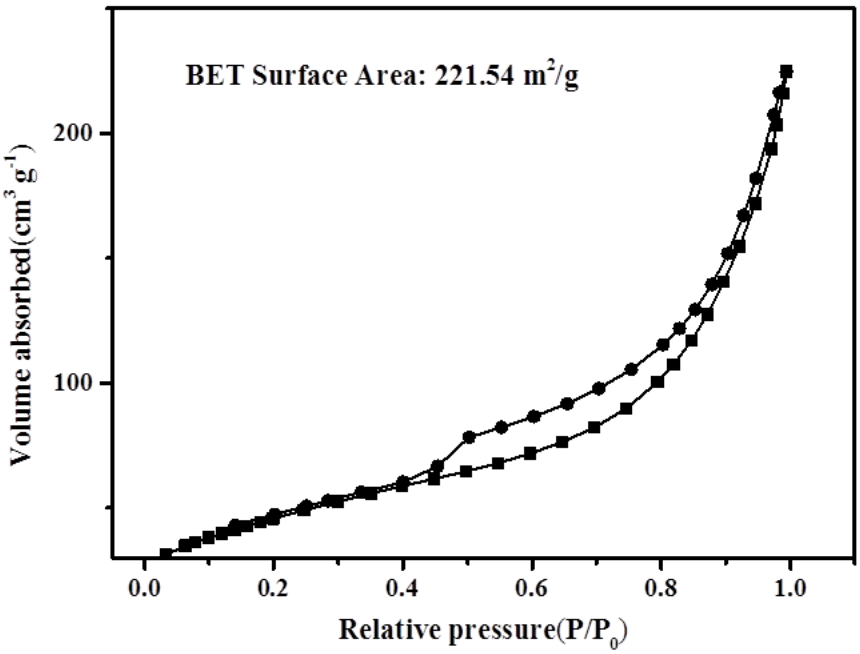

Fig. S8. N_2 absorption/desorption isotherms of CeO_x/CoS@L-CeO_2NRs.

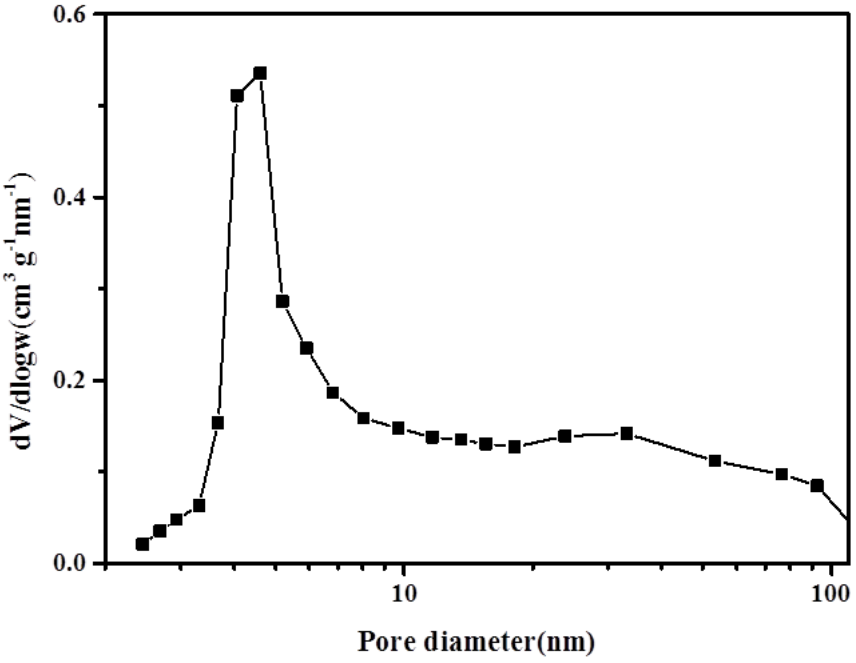

Fig. S9. Pore size distribution of CeO_x/CoS@L-CeO_2NRs.

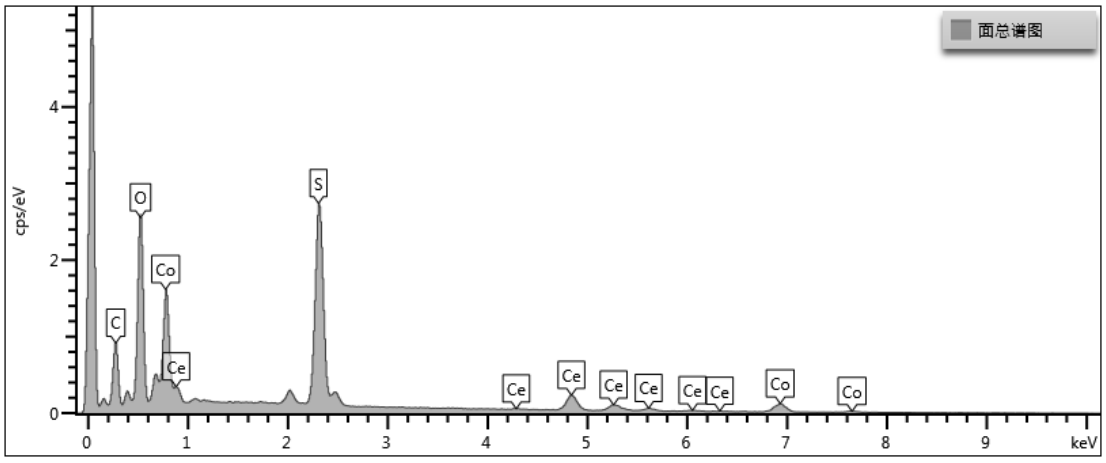

Fig. S10. EDX spectrum of CeO_x/CoS@L-CeO_2NRs.

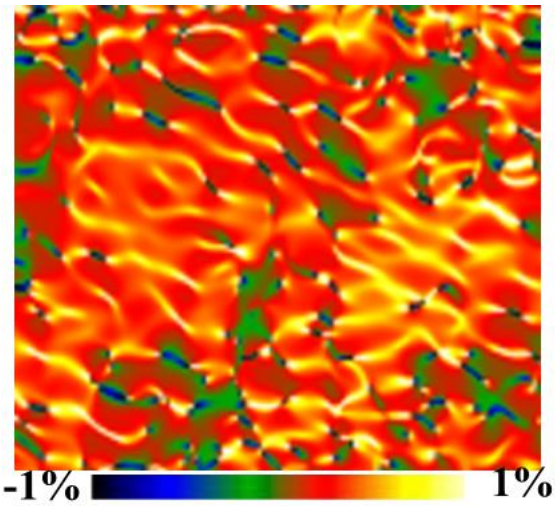

Fig. S11 The strain tensor map generated from the HRTEM image on the surface of CeO_x/CoS polyhedrons using geometric phase analysis.

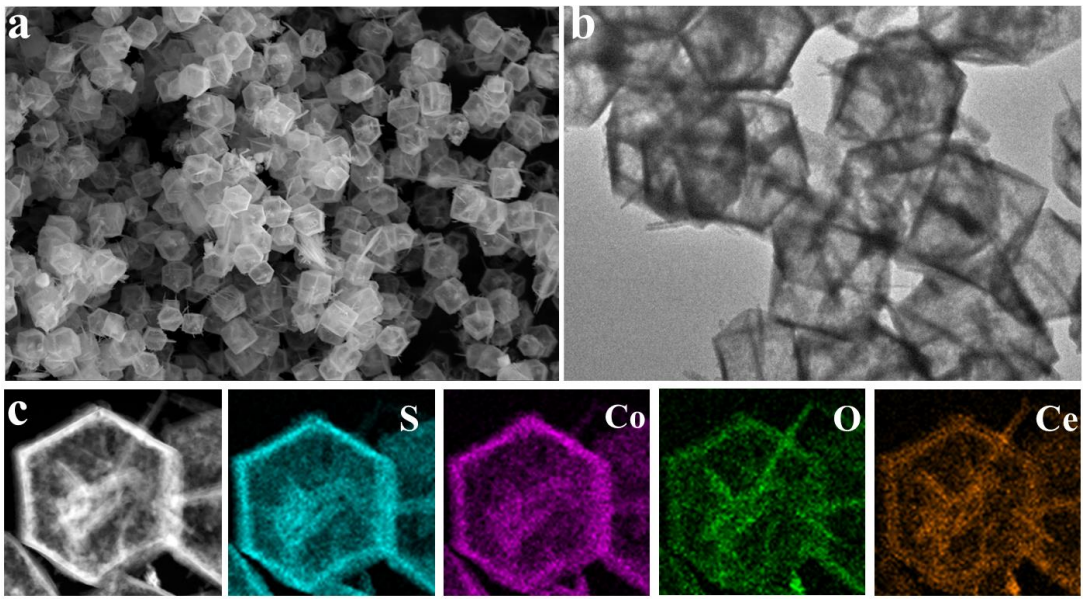

Fig. S12. The SEM and TEM images for CeO_x/CoS@S-CeO_2NRs (a and b). c) Elemental mapping images of CeO_x/CoS@S-CeO_2NRs.

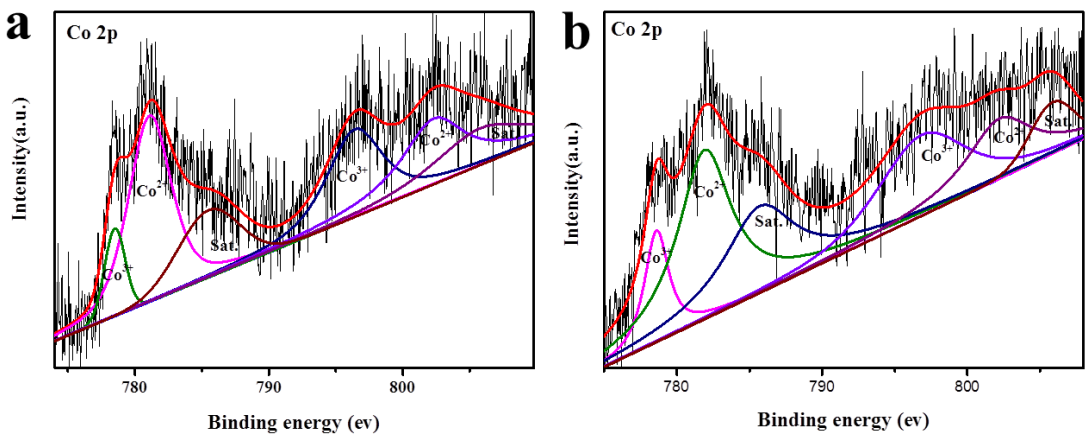

Fig. S13. XPS spectra of Co 2p for CeO_x/CoS@L-CeO_2NRs (a) and CeO_x/CoS@S-CeO_2NRs (b).

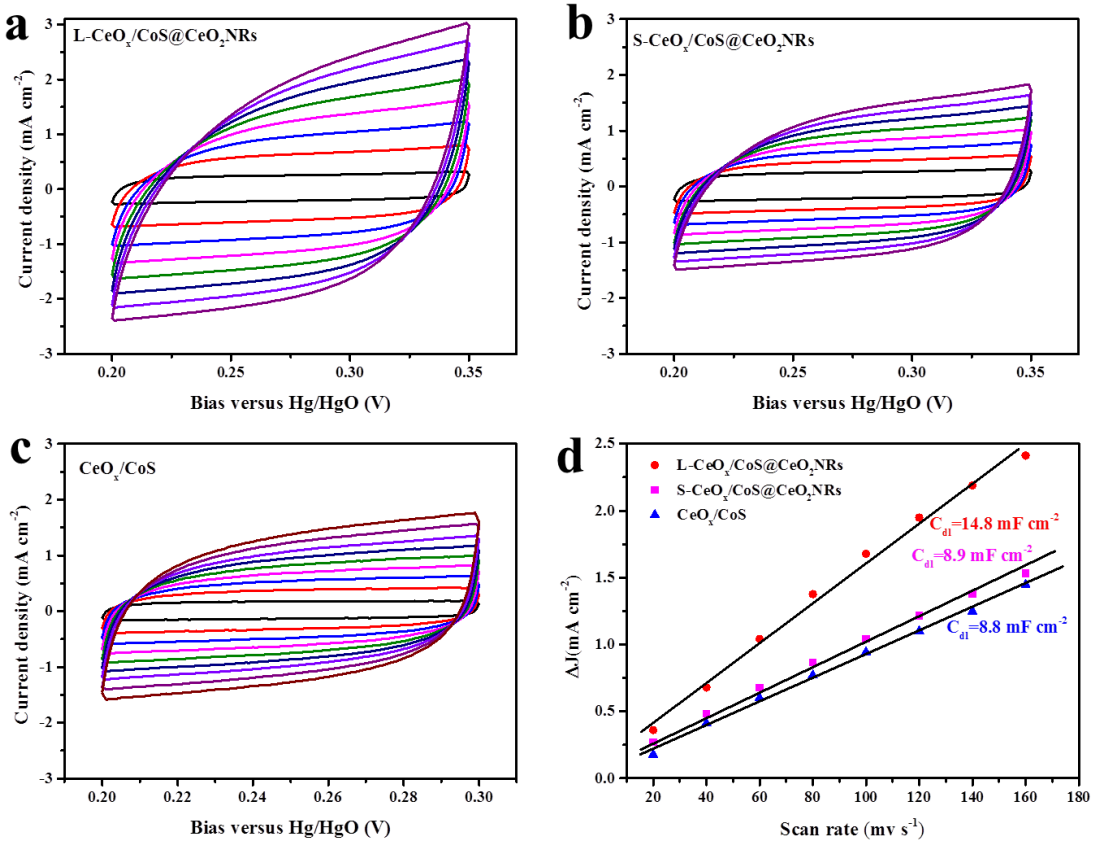

Fig. S14. (a-c).Typical cyclic voltammetry curves of CeO_x/CoS@L-CeO_2NRs, CeO_x/CoS@S-CeO_2NRs and CeO_x/CoS in 1M KOH with different scan rates. d. Capacitive J versus scan rate for CeO_x/CoS@L-CeO_2NRs, CeO_x/CoS@S-CeO_2NRs and CeO_x/CoS.

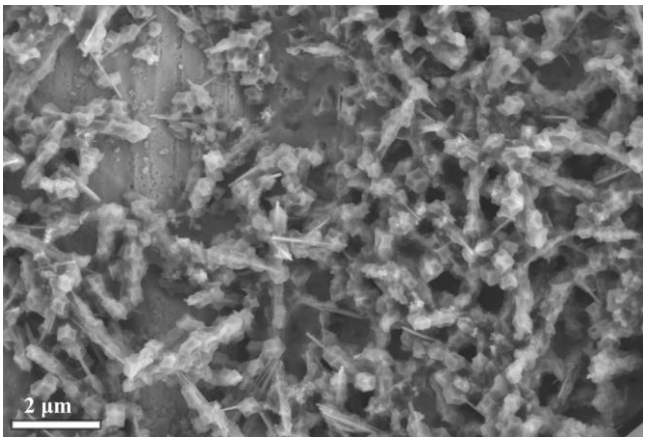

Fig. S15. SEM micrograph of CeO_x/CoS@L-CeO_2NRs after the OER reaction.

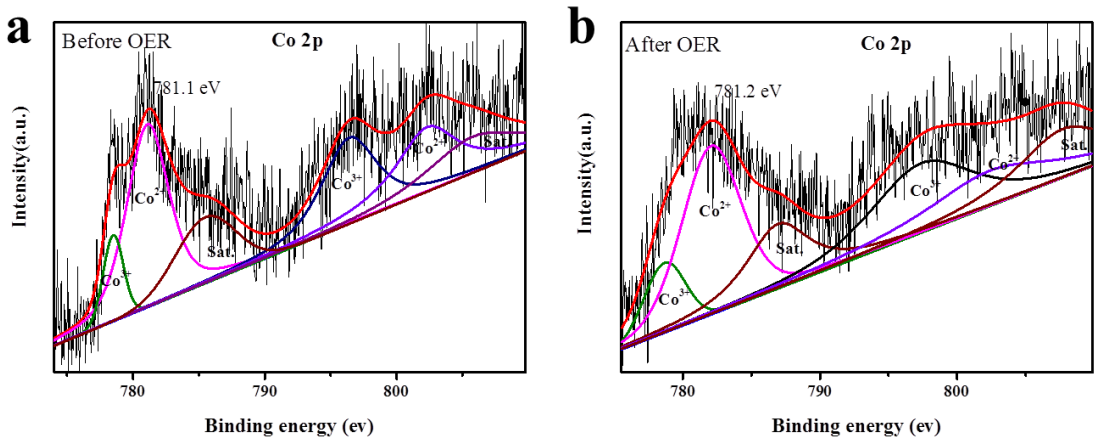

Fig. S16. XPS spectra of Co 2p before and after the OER reaction for CeO_x/CoS@L-CeO_2NRs.

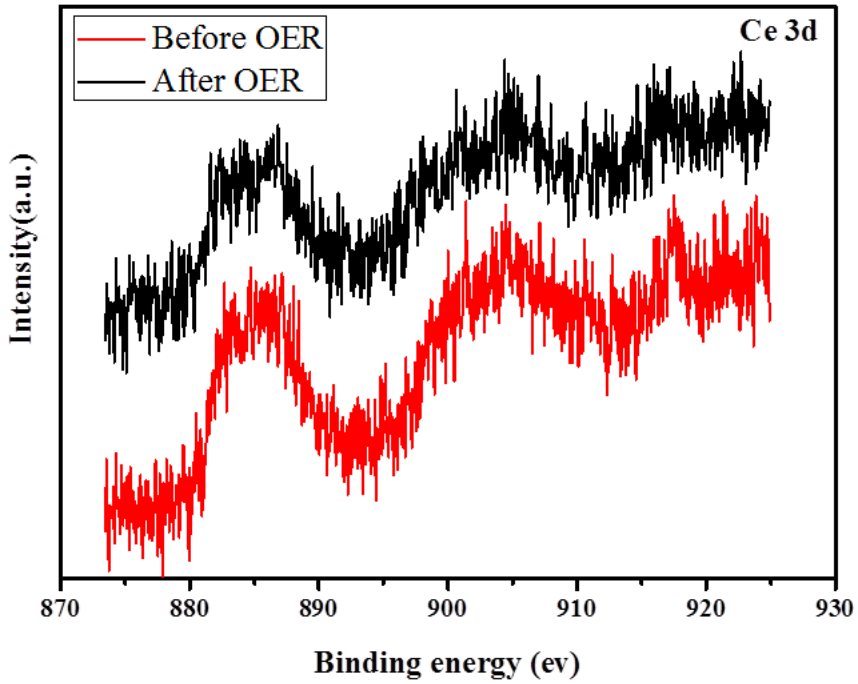

Fig. S17. XPS spectra of Ce 3d before and after the OER reaction for CeO_x/CoS@L-CeO_2NRs.

5. Supplementary Tables

Table S1 Comparison of catalytic performance with reported Co-based catalyst.

Catalyst	Support	Electrolyte	η@10mA cm^{-2} (mV)	Tafel solpe (mV dec^{-1})	Ref.
CoMnP	GC	1M KOH	284	61	J. Am. Chem. Soc. **2016**, 138, 4006.
Co_3O_4/Co-Fe oxide DSNBs	GC	1M KOH	297	61	Adv. Mater. 2018, 1801211.
Co_3S_4@MoS_2	GC	1M KOH	310	59	Chem. Mater. **2017**, 29, 5566-5573.
Co_3O_4/$NiCo_2O_4$	Ni foam	1M KOH	340	88	J. Am. Chem. Soc. **2015**, 137, 5590-5595.
Co-P Film	GC	1M KOH	345	47	Angew. Chem. Int. Ed. **2015**, 54, 6251-6254.
Cobalt Sulfide	Carbon Paper	1M KOH	306	72	ACS Nano. **2016**, 10, 2342-2348.
$NiCo_2O_4$	GC	1M KOH	250	50	J. Am. Chem. Soc. 2018, 140, 13644.
Co_3O_4 NW	CC	1M KOH	320	72	Angew. Chem. Int. Ed. **2015**, 54, 14710.
Co@Co_3O_4/NC	GC	0.1M KOH	410	54.3	Angew. Chem. Int. Ed. **2016**, 55, 4087.
Co9S8@NOSC-900	Ni foam	1M KOH	330	68	Adv. Funct. Mater, **2017**, 27. 1606585.
CoO_x-ZIF	GC	1M KOH	310	70.3	Adv. Funct. Mater. **2017**, 27, 1702546
N-CG-CoO	GC	1M KOH	340	70	Energ. Environ. Sci. 2014, 7, 609-616.
Mn-Co	GC	1M KOH	320	52	Angew. Chem. Int. Edit. **2017**, 56, 2386-2389.
NiCoP/C	GC	1M KOH	330	96	Angew. Chem. Int. Ed. **2017**, 56, 3897-3958.
N-doped	GC	1M KOH	280	82.7	Energ. Environ. Sci. **2016**, 9, 1320-1326.
$Co_{0.9}S_{0.58}P_{0.42}$	GC	1M KOH	266	48	ACS Nano. **2017**, 11, 11031-11040.
$CuCo_2S_4$ nanosheets	GC	1M KOH	310	98	ACS Catal. **2017**, 7, 5871-5879.
A-$CoS_{4.6}O_{0.6}$ PNCs	GC	1M KOH	290	67	Angew. Chem. Int. Ed. **2017**, 56, 4858-4861.
G-FeCoW	Gold Ni foam	1M KOH	190	37	Science**. 2016**, 352, 6583.
N-Co_9S_8/G	RDE	0.1M KOH	410	83	Energy Environ. Sci. **2016**, 9, 1320.
CeO_x/CoS	GC	1M KOH	269	50	Angew.Chem. Int.Ed. 2018, 57,8654.
CeO_x/CoS-@ S-CeO_2NRs	GC	1M KOH	268	48	This work
CeO_x/CoS-@ L-CeO_2NRs	GC	1M KOH	238	42	This work